ARTICLES
https://doi.org/10.1038/s41561-017-0041-0
nature geoscience

Role of polar anticyclones and mid-latitude cyclones for Arctic summertime sea-ice melting

Heini Wernli[1*] and Lukas Papritz[1,2]

Annual minima in Arctic sea-ice extent and volume have been decreasing rapidly since the late 1970s, with substantial interannual variability. Summers with a particularly strong reduction of Arctic sea-ice extent are characterized by anticyclonic circulation anomalies from the surface to the upper troposphere. Here, we investigate the origin of these seasonal circulation anomalies by identifying individual Arctic anticyclones (with a lifetime of typically ten days) and analysing the air mass transport into these systems. We reveal that these episodic upper-level induced Arctic anticyclones are relevant for generating seasonal circulation anomalies. Sea-ice reduction is systematically enhanced during the transient episodes with Arctic anticyclones and the seasonal reduction of sea-ice volume correlates with the area-averaged frequency of Arctic anticyclones poleward of 70° N (correlation coefficient of 0.57). A trajectory analysis shows that these anticyclones result from extratropical cyclones injecting extratropical air masses with low potential vorticity into the Arctic upper troposphere. Our results emphasize the fundamental role of extratropical cyclones and associated diabatic processes in establishing Arctic anticyclones and, in turn, seasonal circulation anomalies, which are of key importance for understanding the variability of summertime Arctic sea-ice melting.

The strong reduction in late summer minimum Arctic sea-ice extent during the last decades is one of the most prominent signals of anthropogenic climate warming due to increased greenhouse gas concentrations[1,2]. This reduction is not linear in time and the decrease seems to be stronger after 1996[3]. Furthermore, the interannual variability is high[4,5], with record-low sea-ice coverage reached in late summers 2007 and 2012 (Supplementary Fig. 1a), and its predictability is surprisingly low, even on relatively short (intraseasonal) timescales[6]. The long-term declining trend of Arctic sea ice is regarded as the main driver of the so-called Arctic amplification (that is, the stronger climate warming in the Arctic compared with that at lower latitudes)[7]. In turn, Arctic amplification leads to a reduced meridional temperature gradient, with potentially important—but so far not well understood—consequences for the dynamics of mid-latitude weather and extreme events[8,9]. This study, however, addresses a potential influence in the opposite direction; that is, the role of extratropical dynamics for the high interannual variability of summertime Arctic sea-ice melting (Supplementary Fig. 1b).

A number of different processes have been suggested that influence summertime Arctic sea-ice melting. It is generally agreed that poleward oceanic heat fluxes play a role, but that the most important processes are atmospheric[10], including, in particular, low-level Arctic clouds[11,12], moisture transport into the Arctic[13], Arctic cyclones[14,15] and seasonal anticyclonic circulation anomalies[16]. Low Arctic clouds reflect shortwave radiation (effectively cooling the surface) and increase downward longwave radiation (warming the surface), with a net cooling effect in summer[12]. In summer 2007, a reduction of cloudiness led to a positive shortwave radiation anomaly and low-level warming in the portion of the Arctic Ocean with strongest sea-ice loss[11,12]. In addition, increasing specific humidity in the Arctic is also expected to have contributed to the loss of sea ice via its impact on longwave radiation[17–19]. Moisture transport into the Arctic is strongly related to extratropical cyclones[20,21]. The direct impact of summertime Arctic cyclones is controversial. On the one hand, indications were found that fewer cyclones throughout summer favour a stronger sea-ice retreat[14], whereas, on the other hand, intense cyclones can accelerate sea-ice reduction, by inducing sea-ice motion[22] or, in particular in late summer, through mechanical break-up and melt due to wind-induced upward ocean heat transport[15].

Arctic anticyclones

In recent years, several studies emphasized the importance of anticyclonic circulation anomalies for the variability of minimum sea-ice extent[16,23]. It was found that the decrease of sea-ice extent was particularly large in summer months with an anomalously anticyclonic mean circulation at 925 hPa (ref. [16]). A recent study[23] revealed the vertically coherent structure of these anticyclonic flow anomalies from the surface to the upper troposphere and quantified, using simulations with an atmospheric general circulation model coupled to a simple ocean–sea-ice model, that up to 60% of the late summer decline of the sea-ice extent since 1979 can be attributed to trends in the summer mean atmospheric circulation. In principle, these seasonal circulation anomalies can affect sea ice in at least two complementary ways. On the one hand, they can lead to an enhanced export of sea ice out of the Arctic (kinematic effect), in particular via the Fram Strait when the centre of the anticyclonic flow anomaly is located over northern Greenland[4,24–26], and subsequent melt outside the Arctic Ocean. On the other hand, anticyclonic anomalies are associated with downwelling motion through most of the troposphere, leading to adiabatic warming and a shift towards lower clouds, eventually leading to increased longwave downward radiation[23] (thermodynamic effect). This effect is amplified by an increase in water vapour in the warm lower atmosphere. The seasonal upper-level anticyclonic circulation anomalies are regarded as manifestations of internal atmospheric variability[23,27] and it has been speculated that teleconnections with the Asian summer monsoon and the tropics are responsible for this internal variability[23,28]. In the following, we shed light on the origin of these seasonal

[1]Institute for Atmospheric and Climate Science, ETH Zurich, Switzerland. [2]Geophysical Institute, University of Bergen and Bjerknes Centre for Climate Research, Bergen, Norway. *e-mail: heini.wernli@env.ethz.ch

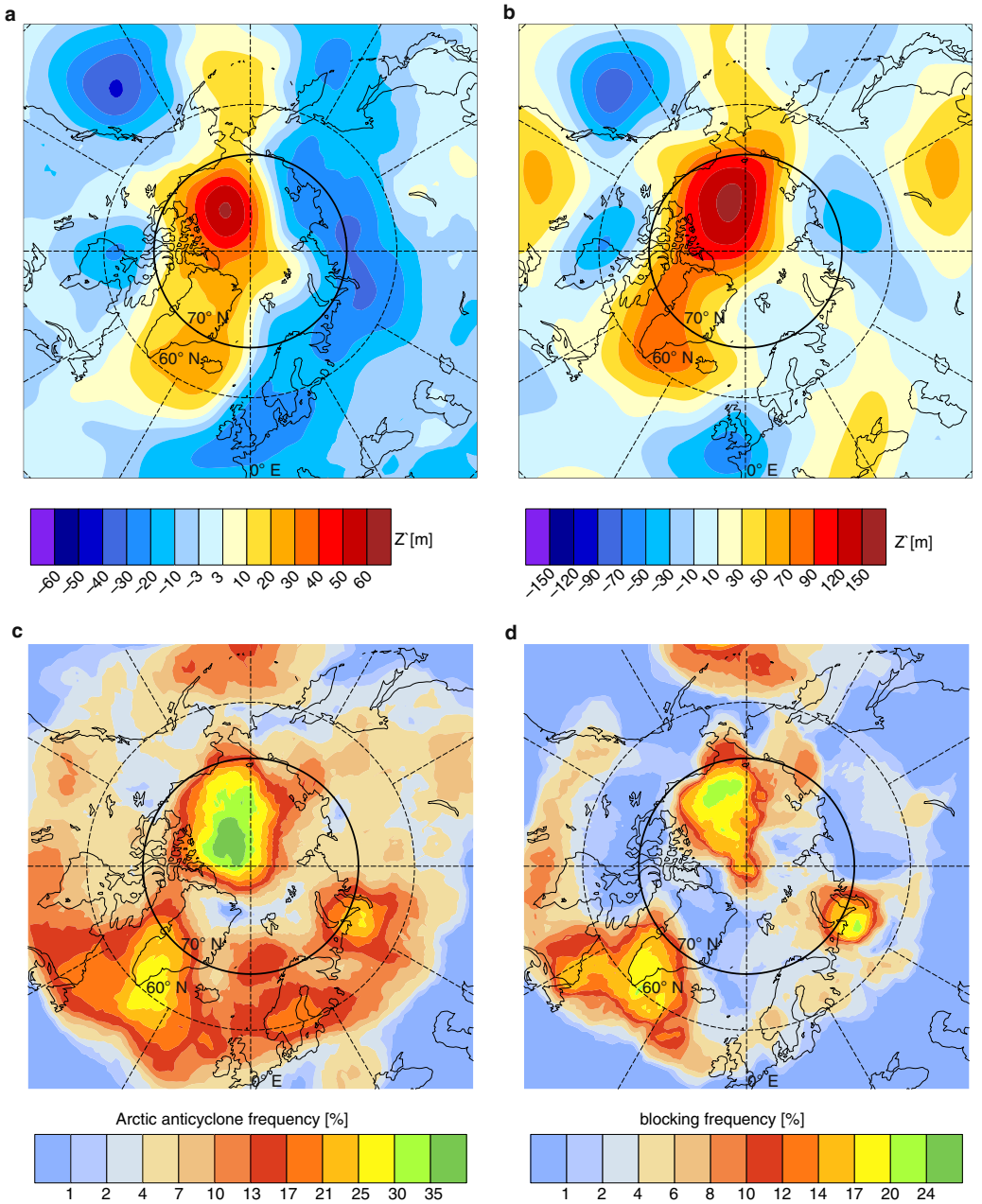

Fig. 1 | Vertically coherent, seasonal geopotential height anomalies are the result of Arctic anticyclones. a,**b**, Seasonal mean geopotential height anomalies Z' (m); at 925 hPa (**a**) and at 300 hPa (**b**). Seasonal geopotential height anomalies have been calculated as deviations from the climatological summer average (1979–2016). **c**, Frequency of Arctic anticyclones. **d**, Frequency of blocks. All fields are for summer (June–August) 2007. See Methods for the definition of Arctic anticyclones and blocks.

circulation anomalies. We show that they result from a few episodic events (with a typical lifetime of ten days) of Arctic anticyclones per summer season, and that these events are intimately related to the injection of extratropical air masses to the Arctic associated with mid-latitude cyclones.

Figure 1 shows circulation anomalies and frequency maps of Arctic anticyclones and blocks (see Methods for identification techniques) for summer 2007. In agreement with previous studies[16,29], this summer is characterized by a low-tropospheric anticyclonic flow anomaly in the Beaufort Sea and central Arctic (Fig. 1a) and weaker cyclonic anomalies in the eastern Arctic. The structure of the seasonal Arctic anticyclonic anomaly is barotropic[23]; that is, Fig. 1b reveals almost the same anomaly pattern at 300 hPa as seen at 925 hPa (Fig. 1a). This flow anomaly configuration is similar to the Arctic dipole[30,31], but shifted towards the west, and it is consistent with an amplified transpolar drift and larger ice loss via the Fram Strait[24]. As an aside, we note that despite these pronounced flow anomalies, the seasonal mean Arctic flow at 300 hPa is cyclonic in all summers (Supplementary Fig. 2). Importantly, the barotropic anticyclonic flow anomaly in the Beaufort Sea in summer 2007 coincides with a region where Arctic anticyclones occurred with a peak frequency of more than 35% (Fig. 1c). This shows that the formation of about three synoptic-scale anticyclones (each with a lifetime of about ten days, see Methods) accounts for the seasonal circulation anomaly. For about two-thirds of their life cycle, these anticyclones are characterized by very strong negative potential vor-

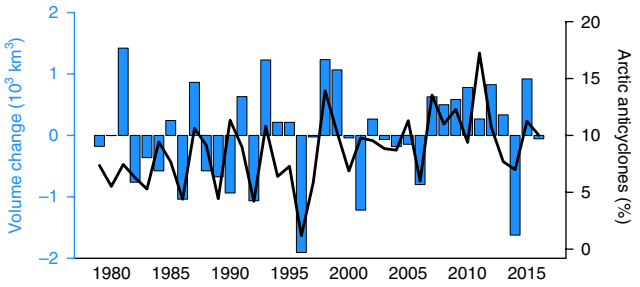

Fig. 2 | Time series of sea-ice volume change anomalies relative to climatology and area-averaged seasonal mean frequency of Arctic anticyclones for the summers of 1979 to 2016. The blue bars show the maximum reduction of sea-ice volume in each summer (that is, between 1 June and 31 August; shown are deviations from the long-term mean), and the black line shows the seasonal mean frequency of Arctic anticyclones averaged north of 70° N.

ticity anomalies (see Supplementary Fig. 3b), such that they are classified as blocks (see peak frequency of about 20% in Fig. 1d). The same agreement between the location of barotropic seasonal mean anticyclonic circulation anomalies and frequency maxima of Arctic anticyclones and blocks is found in other summers (for example, in the summers of 2011 and 2012; Supplementary Figs. 4 and 5).

Impact on sea-ice melting

This striking qualitative agreement between the frequency of Arctic anticyclones and seasonal flow anomalies, and the importance of these anomalies for summertime sea-ice melting[16,23] (see also Supplementary Fig. 6) provide the motivation to consider the time series of the frequency of summertime Arctic anticyclones and the concomitant decrease of sea-ice volume[32] (Fig. 2; we consider sea-ice volume instead of extent because the former is better constrained by thermodynamics and less affected by preconditioning). The increased frequency of anticyclones after 2007 is in line with the general tendency towards a more anticyclonic summertime circulation in the Arctic[16,23]. The summertime sea-ice volume loss is systematically above the long-term mean in the same period, with the only exception being 2014, when the frequency of Arctic anticyclones also featured a minimum. The correlation, however, is also high before the year 2000 when the early summer sea-ice volume was less depleted and, hence, sea ice was less vulnerable in particular to mechanical break-up. Consequently, the two time series have a relatively high Pearson correlation of 0.57 over the entire period. This indicates that the frequency of Arctic anticyclones significantly influences sea-ice variability independently of the total amount of sea ice present in early summer. An inverse analysis, quantifying the probability density of 300 hPa geopotential height anomalies for days with particularly strong sea-ice volume loss, reveals a broadening towards more anticyclonic flow conditions compared with days with low and normal sea-ice volume loss (Supplementary Fig. 7), confirming the important role of strong anticyclones for large daily sea-ice volume reductions.

To better understand the underlying physical processes, we quantify the increase of sea-ice melting during the 126 strongest Arctic anticyclone events. Identifying and quantifying a systematic enhancement of daily sea-ice loss by Arctic anticyclones requires a suitable statistical approach because of the high case-to-case variability of Arctic anticyclones and daily sea-ice volume tendencies. One reason for this high variability is that during such Arctic anticyclone events, sea-ice melt may be enhanced in the region of the Arctic anticyclone, but at the same time it may be reduced due to other factors in the rest of the Arctic, resulting in an overall weak tendency anomaly. A robust signal does emerge, however, when a

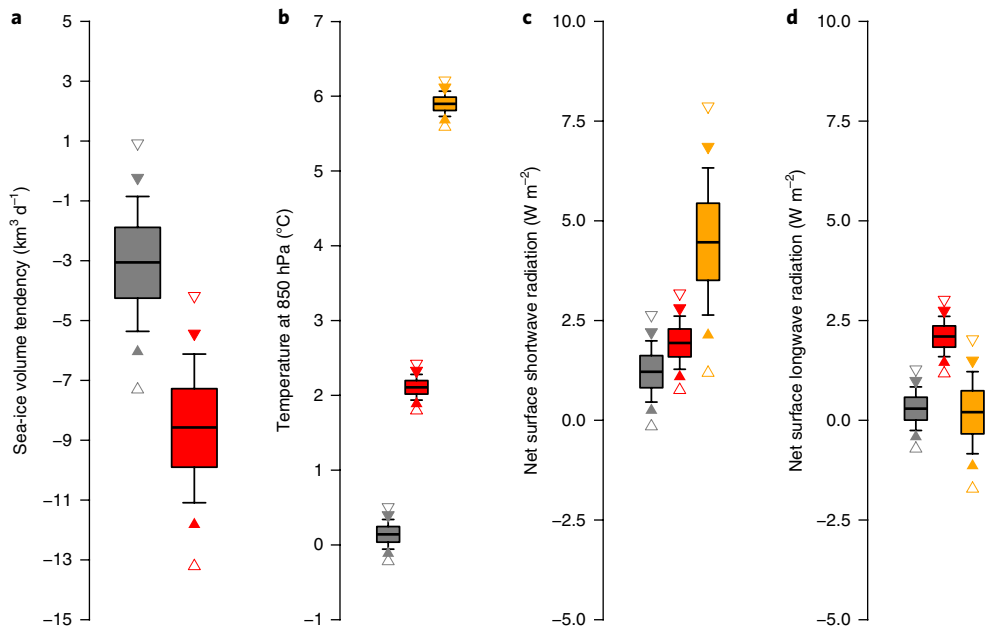

Fig. 3 | Statistical analysis of sea-ice reduction and meteorological parameters related to Arctic anticyclones. a–d, Bootstrapped distribution of mean sea-ice volume tendency anomaly (**a**), temperature anomaly at 850 hPa (**b**), net surface shortwave radiation anomaly (**c**) and net surface longwave radiation anomaly during Arctic anticyclone events (**d**) (see Methods). Sea-ice volume tendency is integrated over the entire Arctic (red), whereas temperature and surface radiation are averaged over all grid points polewards of 70° N with sea-ice concentration greater than 0.2 (red), as well as over grid points additionally collocated with Arctic anticyclones (orange). Reference estimates of the mean values for randomly chosen days are shown in grey. The whiskers, filled triangles and open triangles indicate the 10%, 5% and 1% confidence intervals, respectively. For details about the computation of the confidence intervals and the reference estimates, see Methods.

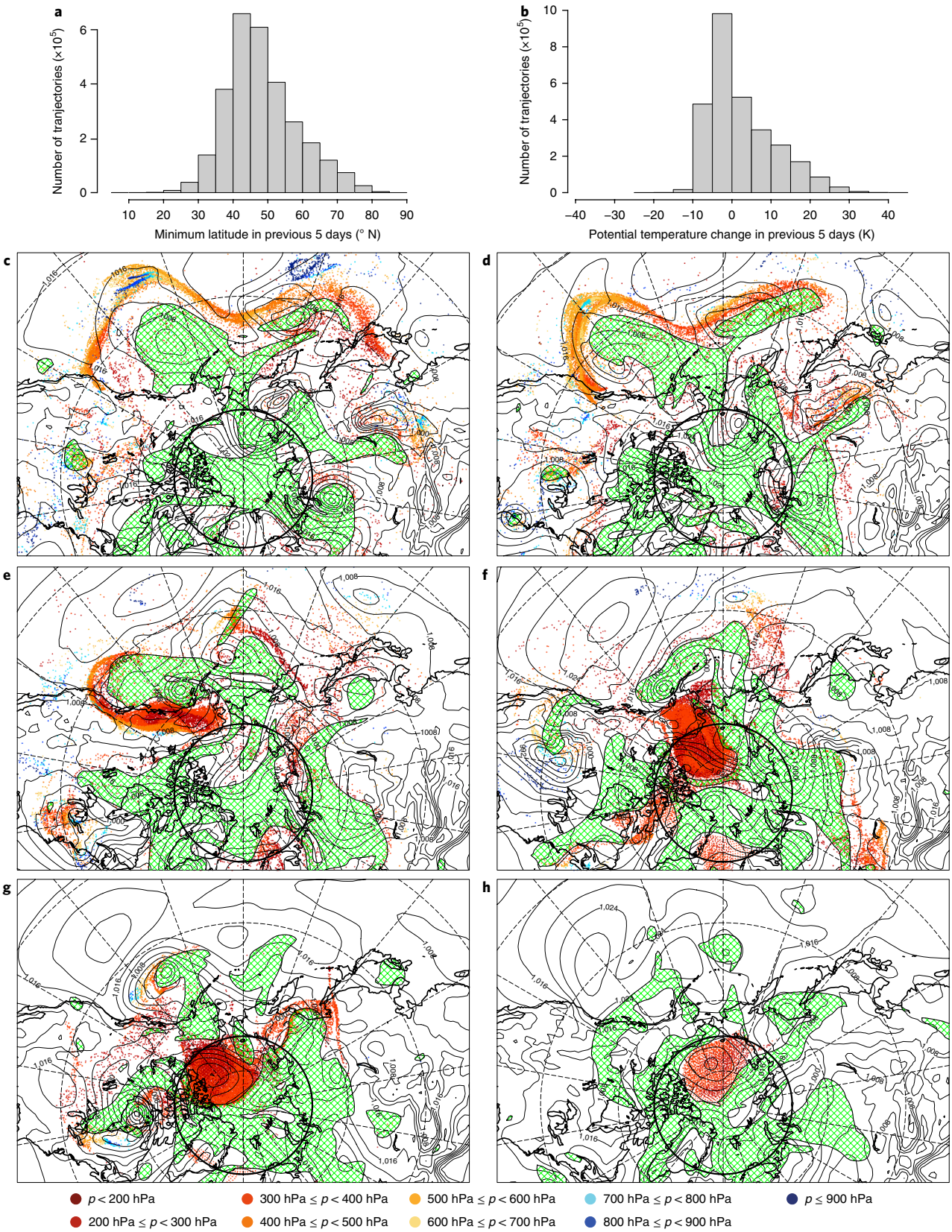

Fig. 4 | Intrusions of extratropical air into the Arctic lead to the formation of Arctic anticyclones. a, Histogram of minimum latitude along all backward trajectories between day −5 and day 0, for all Arctic anticyclones between 1979 and 2015. **b**, Histogram of the change in potential temperature along the backward trajectories between day −5 and day 0, for Arctic anticyclones between 1979 and 2015. **c–h**, Case study of the formation of a prominent Arctic anticyclone in June 2007 showing the dynamical tropopause at 300 hPa (green hatching indicates stratospheric air), sea-level pressure (black contours, every 4 hPa) and the position of trajectories ending in the anticyclone (coloured according to pressure (p); see legend). Fields are shown at 12:00 UTC 2 June (**c**); 12:00 UTC 3 June (**d**); 0:00 UTC 5 June (**e**); 0:00 UTC 07 June (**f**); 0:00 UTC 09 June (**g**); and 0:00 UTC 14 June 2007 (**h**).

statistical bootstrap technique (see Methods) is applied to estimate Arctic sea-ice volume tendency anomalies averaged over many anticyclone events and compared with climatological conditions. In fact, average sea-ice volume loss during Arctic anticyclone events is intensified by about 6 $km^3 d^{-1}$ at the 10% significance level (Fig. 3a). Subsidence within Arctic anticyclones (Supplementary Fig. 8a) induces significant adiabatic warming such that the temperature at 850 hPa above sea ice within Arctic anticyclones is enhanced by almost 6 K in the mean (Fig. 3b). A trajectory analysis (see Methods) confirms that air masses in Arctic anticyclones at 850 hPa are indeed mainly heated within the Arctic by adiabatic descent during the previous two days (Supplementary Fig. 9). The warming and subsidence in the anticyclones result in reduced cloud water content (Supplementary Fig. 8c), and thus enhanced net shortwave radiation at the surface (Fig. 3c). A similar mechanism was found to be relevant for Greenland ice-sheet melting[33]. In addition, and consistent with the results of an earlier study[23], there is also a significant increase in downwelling longwave radiation during Arctic anticyclone events (Fig. 3d). This increase, however, is limited to the region outside Arctic anticyclones, where the reduction in cloud water content is smaller than inside but total column water vapour is significantly enhanced (Supplementary Fig. 8b,c). The case study shown in Supplementary Figs. 10–14 indicates that the uneven changes of total column vapour inside and outside Arctic anticyclones are due to the import of moist air masses into the Arctic along the periphery of Arctic anticyclones, where the meridional transport is strongest. As a consequence, surface longwave radiation anomalies are strongest at the edge and outside of Arctic anticyclones, whereas surface shortwave radiation anomalies peak in the central area of the anticyclones where subsidence is strongest. Supplementary Fig. 15 illustrates the robustness of our findings for stronger and weaker anticyclones.

Formation of Arctic anticyclones

Finally, we address the formation mechanism of Arctic anticyclones by studying large ensembles of backward trajectories from all anticyclones at 300 hPa. The trajectories reveal that air masses involved in Arctic anticyclones are injected from mid-latitudes into the Arctic upper troposphere (Fig. 4a). These injections occur largely in association with extratropical cyclones: about half of the air masses experience substantial ascent and latent heating up to more than 20 K during poleward transport, whereas the other half moves into the Arctic nearly along isentropic surfaces while experiencing moderate radiative cooling of a few K (Fig. 4b). Some of the ascending air parcels reside even in the subtropical oceanic boundary layer about ten days before contributing to the formation of an Arctic anticyclone. With their region of origin, strong ascent and latent heating, they correspond to so-called warm conveyor belts—strongly diabatic airstreams within extratropical cyclones[34,35] (see Methods) that have been shown to be of central importance for the amplification of mid-latitude upper-level ridges and blocks[35–37]. The dynamical relevance of diabatic airstreams is mainly due to their contribution to the formation of strongly negative potential vorticity anomalies in the upper troposphere[35,36]. Our findings reveal that such airstreams and their associated negative potential vorticity anomalies (Supplementary Fig. 3b) also play an essential role in the formation of Arctic anticyclones.

The formation of an Arctic anticyclone and the role of latent heating are exemplarily portrayed in Fig. 4c–h for an event in early June 2007 (additional fields for this episode are shown in Supplementary Figs. 10–14). Fig. 4c shows many air parcels over the North Pacific between 30–50° N on 2 June that will form the upper-tropospheric part of an Arctic anticyclone a few days later. Many of them are in the mid-troposphere and follow the flow imposed by the trough–ridge pattern. Some air parcels are located in the oceanic boundary layer (blue colours), south of developing extratropical cyclones. During the following days (Fig. 4d,e), the low-tropospheric air parcels experience intense latent heating as they rise within the North Pacific cyclones' warm conveyor belts, and most of them enter the Arctic between 5 and 9 June over North America as part of the prominent ridge downstream of the cyclone in the Gulf of Alaska (Fig. 4e–g). On 9 June, a weaker plume of extratropical air enters the Arctic over Siberia and merges with the well-established Arctic anticyclone in the Beaufort Sea (Fig. 4g,h). The sea-level pressure and upper-level potential vorticity contours demonstrate the barotropic nature of this exemplary Arctic anticyclone (Fig. 4g,h).

In conclusion, our analyses reveal the importance of transient, synoptic-scale polar anticyclones for Arctic summertime sea-ice melting. During these anticyclone events, downwelling leads to adiabatic warming and reduced cloudiness, as well as enhanced net surface radiation—within the anticyclones due to increased shortwave fluxes and in their periphery due to enhanced longwave radiation associated with an increase in water vapour. Anomalous and sustained low-level winds associated with these anticyclones may also contribute to enhanced export and mechanical break-up of thin ice[16]. The previously documented importance of seasonal circulation anomalies for the interannual variability of summertime sea-ice melting[16,23] is therefore, as quantified here, to a large extent caused by variations in the frequency of episodic Arctic anticyclones.

Another important conclusion is that these anticyclones are formed through injections of air masses with low potential vorticity into the Arctic upper troposphere by lower latitude cyclones. About half of this transport is associated with intense latent heating in the cyclones' cloud systems, further corroborating the important role of diabatic processes for atmospheric dynamics[36–38]. Cyclone activity in Northern Hemisphere summer is high over both the oceans and continents[39] and therefore air mass injections into the Arctic occur at all longitudes, with maxima over Siberia, North America and Europe (Supplementary Fig. 16). This contributes to the observed large variability in the location of summer mean anticyclonic circulation anomalies and their impact on late summer sea-ice extent[5]. In line with a previous study[27], our results emphasize the role of transient synoptic-scale processes for establishing seasonal flow anomalies that are, in this case, of direct relevance for the interannual variability of summertime Arctic sea-ice melting. The realistic representation of Arctic anticyclone formation in global climate models is thus an essential prerequisite for studying the interannual variability of Arctic sea ice in the future warmer climate.

Methods

Methods, including statements of data availability and any associated accession codes and references, are available at https://doi.org/10.1038/s41561-017-0041-0.

Received: 22 June 2017; Accepted: 30 November 2017;
Published online: 15 January 2018

References

1. Simmonds, I. Comparing and contrasting the behaviour of Arctic and Antarctic sea ice over the 35 year period 1979–2013. *Ann. Glaciol.* **56**, 18–28 (2015).
2. Kay, J. E., Holland, M. M. & Jahn, A. Inter-annual to multi-decadal Arctic sea ice extent trends in a warming world. *Geophys. Res. Lett.* **38**, L15708 (2011).
3. Ogi, M. & Rigor, I. G. Trends in Arctic sea ice and the role of atmospheric circulation. *Atmos. Sci. Lett.* **14**, 97–101 (2013).
4. Wettstein, J. J. & Deser, C. Internal variability in projections of twenty-first century Arctic sea ice loss: role of the large-scale atmospheric circulation. *J. Clim.* **27**, 527–550 (2014).
5. Serreze, M. C., Stroeve, J., Barrett, A. P. & Boisvert, L. N. Summer atmospheric circulation anomalies over the Arctic Ocean and their influences on September sea ice extent: a cautionary tale. *J. Geophys. Res. Atmos.* **121**, 11463–11485 (2016).

6. Stroeve, J., Hamilton, L. C., Bitz, C. M. & Blanchard-Wrigglesworth, E. Predicting September sea ice: Ensemble skill of the SEARCH Sea Ice Outlook 2008–2013. *Geophys. Res. Lett.* **41**, 2411–2418 (2014).
7. Screen, J. A. & Simmonds, I. The central role of diminishing sea ice in recent Arctic temperature amplification. *Nature* **464**, 1334–1337 (2010).
8. Cohen, J. et al. Recent Arctic amplification and extreme mid-latitude weather. *Nat. Geosci.* **7**, 627–637 (2014).
9. Barnes, E. A., & Screen, J. A. The impact of Arctic warming on the midlatitude jet-stream: Can it? Has it? Will it?. *WIREs Clim. Change* **6**, 277–286 (2016).
10. Döscher, R., Vihma, T. & Maksimovich, E. Recent advances in understanding the Arctic climate system state and change from a sea ice perspective: a review. *Atmos. Chem. Phys.* **14**, 13571–13600 (2014).
11. Kay, J. E., L'Ecuyer, T., Gettelman, A., Stephens, G. & O'Dell, C. The contribution of cloud and radiation anomalies to the 2007 Arctic sea ice extent minimum. *Geophys. Res. Lett.* **35**, L08503 (2008).
12. Kay, J. E. & L'Ecuyer, T. Observational constraints on Arctic Ocean clouds and radiative fluxes during the early 21st century. *J. Geophys. Res. Atmos.* **118**, 7219–7236 (2013).
13. Graversen, R. G., Mauritsen, T., Drijfhout, S., Tjernström, M. & Mårtensson, S. Warm winds from the Pacific caused extensive Arctic sea-ice melt in summer 2007. *Clim. Dynam.* **36**, 2103–2112 (2010).
14. Screen, J. A., Simmonds, I. & Keay, K. Dramatic interannual changes of perennial Arctic sea ice linked to abnormal summer storm activity. *J. Geophys. Res.* **116**, D15105 (2011).
15. Zhang, J., Lindsay, R., Schweiger, A. & Steele, M. The impact of an intense summer cyclone on 2012 Arctic sea ice retreat. *Geophys. Res. Lett.* **40**, 720–726 (2013).
16. Ogi, M. & Wallace, J. M. The role of summer surface wind anomalies in the summer Arctic sea ice extent in 2010 and 2011. *Geophys. Res. Lett.* **39**, L09704 (2012).
17. Gong, T., Feldstein, S. & Lee, S. The role of downward infrared radiation in the recent Arctic winter warming trend. *J. Clim.* **30**, 4937–4949 (2017).
18. Woods, C. & Caballero, R. The role of moist intrusions in winter Arctic warming and sea ice decline. *J. Clim.* **29**, 4473–4485 (2016).
19. Lee, H. J. et al. Impact of poleward moisture transport from the North Pacific on the acceleration of sea ice loss in the Arctic since 2002. *J. Clim.* **30**, 6757–6769 (2017).
20. Jakobson, E. & Vihma, T. Atmospheric moisture budget in the Arctic based on the ERA-40 reanalysis. *Int. J. Climatol.* **30**, 2175–2194 (2010).
21. Doyle, S. H. et al. Amplified melt and flow of the Greenland ice sheet driven by late-summer cyclonic rainfall. *Nat. Geosci.* **8**, 647–653 (2015).
22. Belchansky, G. I., Douglas, D. C. & Platanov, N. G. Duration of the Arctic sea ice melt season: Regional and interannual variability, 1979–2001. *J. Clim.* **17**, 67–80 (2004).
23. Ding, Q. et al. Influence of high-latitude atmospheric circulation changes on summertime Arctic sea ice. *Nat. Clim. Change* **7**, 289–296 (2017).
24. Kwok, R. Outflow of Arctic Ocean sea ice into the Greenland and Barents Seas: 1979–2007. *J. Clim.* **22**, 2438–2457 (2009).
25. Tsukernik, M., Deser, C., Alexander, M. & Tomas, R. Atmospheric forcing of Fram Strait sea ice export: a closer look. *Clim. Dynam.* **35**, 1349–1360 (2010).
26. Smedsrud, L. H., Halvorsen, M. H., Stroeve, J. C., Zhang, R. & Kloster, K. Fram Strait sea ice export variability and September Arctic sea ice extent over the last 80 years. *Cryosphere* **11**, 65–79 (2017).
27. Davies, H. C. Weather chains during the 2013/2014 winter and their significance for seasonal prediction. *Nat. Geosci.* **8**, 833–837 (2015).
28. Grunseich, G. & Wang, B. Arctic sea ice patterns driven by the Asian summer monsoon. *J. Clim.* **29**, 9097–9112 (2016).
29. Ogi, M., Rigor, I. G., McPhee, M. G. & Wallace, J. M. Summer retreat of Arctic sea ice: role of summer winds. *Geophys. Res. Lett.* **35**, L24701 (2008).
30. Watanabe, E., Wang, J., Sumi, A. & Hasumi, H. Arctic dipole anomaly and its contribution to sea ice export from the Arctic Ocean in the 20th century. *Geophys. Res. Lett.* **33**, L23703 (2006).
31. Wang, J. et al. Is the dipole anomaly a major driver to record lows in Arctic summer sea ice extent? *Geophys. Res. Lett.* **36**, L05706 (2009).
32. Schweiger, A., Lindsay, R., Zhang, J., Steele, J. & Stern, H. Uncertainty in modeled Arctic sea ice volume. *J. Geophys. Res.* **116**, C00D06 (2011).
33. Hofer, S., Tedstone, A. J., Fettweis, X. & Bamber, J. L. Decreasing cloud cover drives the recent mass loss on the Greenland Ice Sheet. *Sci. Adv.* **3**, e1700584 (2017).
34. Browning, K. A. in *Extratropical Cyclones: The Erik Palmén Memorial Volume* (eds Newton, C. W. & Holopainen E. O.) 129–153 (American Meteorological Society, Boston, 1990).
35. Madonna, E., Wernli, H., Joos, H. & Martius, O. Warm conveyor belts in the ERA-Interim data set (1979-2010). Part I: Climatology and potential vorticity evolution. *J. Clim.* **27**, 3–26 (2014).
36. Grams, C. M. et al. The key role of diabatic processes in modifying the upper-tropospheric wave guide: a North Atlantic case-study. *Q. J. R. Meteorol. Soc.* **137**, 2174–2193 (2011).
37. Pfahl, S., Schwierz, C., Croci-Maspoli, M., Grams, C. M. & Wernli, H. Importance of latent heat release in ascending air streams for atmospheric blocking. *Nat. Geosci.* **8**, 610–614 (2015).
38. Joos, H. & Wernli, H. Influence of microphysical processes on the potential vorticity development in a warm conveyor belt: a case study with the limited area model COSMO. *Q. J. R. Meteorol. Soc.* **138**, 407–418 (2012).
39. Wernli, H. & Schwierz, C. Surface cyclones in the ERA40 data set (1958–2001). Part I: novel identification method and global climatology. *J. Atmos. Sci.* **63**, 2486–2507 (2006).

Acknowledgements

L.P. acknowledges funding from the Swiss National Science Foundation (SNSF), Grants P2EZP2_162267 and P300P2_174307. We are very grateful for the technical support from and discussions with H. Binder, M. Boettcher, C. Grams, S. Pfahl and M. Sprenger (all at ETH Zurich) and N. Blaser (UiB). Input from T. Schneider (Caltech) was very helpful for considering surface radiation anomalies associated with Arctic anticyclones.

Author contributions

H.W. initiated this study and calculated the trajectories. L.P analysed the PIOMAS data and performed the statistical analyses. Both authors discussed the results and wrote the manuscript.

Competing interests

The authors declare no competing financial interests.

Additional information

Supplementary information is available for this paper at https://doi.org/10.1038/s41561-017-0041-0.

Reprints and permissions information is available at www.nature.com/reprints.

Correspondence and requests for materials should be addressed to H.W.

Publisher's note: Springer Nature remains neutral with regard to jurisdictional claims in published maps and institutional affiliations.

Methods

Sea-ice volume tendencies. Daily anomalies of Arctic sea-ice volume tendency are computed from integrated sea-ice volume estimates of the Pan-Arctic Ice-Ocean Modeling and Assimilation System version 2.1 (PIOMAS[32]; data were downloaded on 29 September 2016 from http://psc.apl.uw.edu/research/projects/arctic-sea-ice-volume-anomaly/data/). Anomalies are defined as deviations from the one-month running mean. PIOMAS does not provide two-dimensional fields of sea-ice volume but spatially integrated scalar values of total Arctic sea-ice volume in cubic metres. PIOMAS comprises coupled sea ice and ocean models driven by atmospheric forcing from the National Centers for Environmental Prediction/National Center for Atmospheric Research (NCEP/NCAR) reanalysis and, at the domain boundary at 48° N, by a globally integrated ice–ocean model. PIOMAS assimilates sea-ice concentrations from satellites and sea surface temperature over ice-free regions from the NCEP/NCAR reanalysis[40]. A validation of the model against independent field measurements, observations from Navy submarines, and moorings, as well as satellite-retrieved sea-ice thickness data has been undertaken previously[32]. In that study, it was found that PIOMAS tends to locally overestimate the thickness of thin ice and underestimate that of thick ice with an uncertainty of total ice volume in March and October of about 10%. Despite the uncertainties in the estimates from PIOMAS, using sea-ice volume to quantify the impact of anticyclonic circulation anomalies on Arctic sea ice on a day-to-day basis has important advantages compared with sea-ice extent. First, changes in sea-ice volume are directly linked to the energy balance, whereas sea-ice extent is more susceptible to thermodynamic and wind forcing when the ice cover is particularly thin[41]. Second, satellite-derived daily sea-ice concentrations, forming the basis for daily sea-ice extent calculations, are subject to spurious fluctuations, especially during the melt season, due to changes in emissivity and weather effects[42], whereas the PIOMAS model provides a physically constrained time series of daily values, which is thus more consistent with the forcing. Third, continuous daily sea-ice extent observations are not available prior to 1988, while the PIOMAS time series extends back to 1979, thus allowing for a more robust longer-term statistical analysis. In addition, the statistical robustness and the consistency with the atmospheric forcings lend strong support to the reliability of the mechanisms identified in this study using PIOMAS data.

Identification of Arctic anticyclones. Data are obtained from the ERA-Interim reanalysis of the European Centre for Medium-Range Weather Forecasts[43] for the period 1979–2016 on a global 1° x 1° longitude–latitude grid.

For each six-hourly time step, Arctic anticyclones are identified as areas poleward of 70° N where 300 hPa geopotential height exceeds its climatological (1979–2016) one-month running mean by at least 200 m. Using this definition, the time series X of the fraction of Arctic sea ice (delimited by a sea-ice concentration in ERA-Interim ≥0.2) collocated with an Arctic anticyclone is computed. Arctic anticyclone events with a potentially strong impact on sea ice are thus defined as local maxima of the so obtained daily averaged time series ($<X>$) with $<X>$ exceeding 0.2 (126 events, see Fig. 3). With this definition of Arctic anticyclone events, at least 20% of the then existing Arctic sea-ice area is co-located with an anticyclone. Consecutive maxima are de-clustered by selecting the largest maximum within a four-day moving window. To test the sensitivity to the choice of threshold, two additional sets of events with different amplitude ranges are considered; that is, strong events ($<X>$ larger than 0.3; 68 events) and weak-to-strong events ($<X>$ larger than 0.1; 245 events). With a simple tracking algorithm, we found that the typical lifetime of an Arctic anticyclone is a bit more than a week.

Identification of Arctic blocks. Atmospheric blocks are identified with an algorithm based on anomalies (from the monthly climatological mean) of vertically averaged potential vorticity between 500 and 150 hPa. A block is defined as a region with a negative potential vorticity anomaly of −1.3 pvu (potential vorticity unit; 1 pvu = 10^{-6} K kg^{-1} m^2 s^{-1}) or less and a lifetime of at least 5 days[44,45].

Statistical bootstrap method. To assess the robustness of the mean sea-ice volume tendency anomaly during Arctic anticyclone events (see above), a bootstrap distribution is computed. The main idea is to obtain a statistical distribution of the mean tendency for the 126 Arctic anticyclone events, by randomly re-sampling 10^5 times the 126 events with repetitions and computing the mean for each of these 10^5 samples, which yields the red distribution in Fig. 3a. To compare the probabilistic estimate for days with Arctic anticyclones with an estimate of the mean sea-ice volume tendency during normal climatological conditions, 10^5 samples of 126 randomly chosen days are drawn from all days, which yields the grey distribution of the sample mean values in Fig. 3a. The random samples are selected so as to preserve intraseasonal variations in the frequency of Arctic anticyclone events.

The same statistical analysis is also performed for ERA-Interim temperature at 850 hPa, vertical velocity at 700 hPa, relative vorticity at 500 hPa, total column water vapour and total column cloud water, as well as net shortwave and longwave surface radiation. These quantities are averaged over the entire area covered with sea ice (sea-ice concentration ≥0.2). For relative vorticity at 500 hPa, absolute values are considered, whereas for all other quantities anomalies with respect to the climatological one-month running mean are used. In addition, for Arctic anticyclone events, averages are computed over the restricted area where sea ice and Arctic anticyclones are collocated (orange distributions in Fig. 3b–d). For the reference estimates for randomly chosen days, spatial averages are taken over the sea-ice-covered region.

All statistical distributions of sea-ice tendency and atmospheric variables are displayed in the form of box-and-whisker plots, where whiskers, filled and empty triangles indicate the 90th and 10th, 95th and 5th, and 99th and 1st percentiles of the distributions, respectively. Therefore, two distributions can be regarded as different at the 10% significance level if their whiskers do not overlap, and similarly, they are different at the 1% significance level if, for example, the 1st percentile triangle of one distribution is above the 99th percentile triangle of the other.

Trajectory calculations. Three-dimensional kinematic ten-day backward trajectories are calculated from a regular grid at 300 hPa covering a summertime Arctic anticyclone, with grid points every 80 km, at each 6-h time step using ERA-Interim wind fields and the Lagrangian analysis tool[46,47]. In total, this yields almost 3,000,000 trajectories in the 37-year period from 1979 to 2015. In addition to the air parcel location, potential temperature is traced along the trajectories, which allows determination of the integrated diabatic heating along the trajectories.

Warm conveyor belts and latent heating in airstreams. Warm conveyor belts are coherently ascending moist airstreams in extratropical cyclones. They typically rise from the oceanic boundary layer to the upper troposphere within 1–2 days and thereby move several thousand kilometres poleward and produce elongated bands of clouds, latent heating and precipitation[34]. They can be objectively identified as the strongest ascending air parcels in extratropical cyclones and the associated latent heating exceeds 20 K (refs [35,46]). Warm conveyor belts are flow systems with intense interactions of clouds and atmospheric dynamics[38,48], not least because they transport air with low potential vorticity to the level of the mid-latitude jet stream[46,49] (see also Supplementary Fig. 3a), which significantly impacts the evolution of Rossby waves[36,50] and the formation of atmospheric blocks[37]. In this study, we find that warm conveyor belts and weaker variants of these moist airstreams are also strongly involved in the formation of Arctic anticyclones.

Code availability. The software LAGRANTO to calculate the trajectories can be downloaded from http://www.lagranto.ethz.ch. All other codes are available from the authors upon request.

Data availability. The ERA-Interim data can be obtained from the ECMWF data server (https://software.ecmwf.int/wiki/display/WEBAPI/Access+ECMWF+Public+Datasets). The PIOMAS sea-ice volume data are available at http://psc.apl.uw.edu/research/projects/arctic-sea-ice-volume-anomaly/data and the daily NSIDC sea-ice extent data are available at http://nsidc.org/data/seaice_index/archives.html.

References

40. Zhang, J. & Rothrock, D. A. Modeling global sea ice with a thickness and enthalpy distribution model in generalized curvilinear coordinates. *Mon. Weath. Rev.* **131**, 845–861 (2003).
41. Maslanik, J. A. et al. A younger, thinner Arctic ice cover: Increased potential for rapid, extensive sea-ice loss. *Geophys. Res. Lett.* **34**, L24501 (2007).
42. Comiso, J. C. & Nishio, F. Trends in the sea ice cover using enhanced and compatible AMSR-E, SSM/I, and SMMR data. *J. Geophys. Res.* **113**, C02S07 (2008).
43. Dee, D. P. et al. The ERA-Interim reanalysis: configuration and performance of the data assimilation system. *Q. J. R. Meteorol. Soc.* **137**, 553–597 (2011).
44. Schwierz, C., Croci-Maspoli, M. & Davies, H. C. Perspicacious indicators of atmospheric blocking. *Geophys. Res. Lett.* **31**, L06125 (2004).
45. Croci-Maspoli, M., Schwierz, C. & Davies, H. C. A multifaceted climatology of atmospheric blocking and its recent linear trend. *J. Clim.* **20**, 633–649 (2007).
46. Wernli, H. & Davies, H. C. A Lagrangian-based analysis of extratropical cyclones. I: The method and some applications. *Q. J. R. Meteorol. Soc.* **123**, 467–489 (1997).
47. Sprenger, M. & Wernli, H. The LAGRANTO Lagrangian analysis tool – version 2.0. *Geosci. Model Dev.* **8**, 2569–2586 (2015).
48. Martinez-Alvarado, O. et al. The dichotomous structure of the warm conveyor belt. *Q. J. R. Meteorol. Soc.* **140**, 1809–1824 (2014).
49. Methven, J. Potential vorticity in warm conveyor belt outflow. *Q. J. R. Meteorol. Soc.* **141**, 1065–1071 (2015).
50. Gray, S. L., Dunning, C. M., Methven, J., Masato, G. & Chagnon, J. M. Systematic model forecast error in Rossby wave structure. *Geophys. Res. Lett.* **41**, 2979–2987 (2014).